

Effect of Temperature on the Corrosion Behavior of API X80 Steel Pipeline

Okonkwo Paul C^{1*}, Essam Ahmed², A.M.A. Mohamed^{1,2,*}

¹ Qatar University, Center of Advanced Materials, 2713 Doha, Qatar

² Department of Metallurgical and Materials Engineering, Faculty of Petroleum and Mining Engineering, Suez University, 43721 Suez, Egypt,

*E-mail: paulokonkwo@qu.edu.qa

Received: 22 June 2015 / *Accepted:* 11 August 2015 / *Published:* 4 November 2015

The electrochemical behavior of API X80 pipeline steel in 3.5% of NaCl solution containing different concentrations of H₂S at different temperatures was investigated. Corrosion behavior of the API X 80 steel material was evaluated using electrochemical impedance spectroscopy and potentiodynamic polarization measurements. The profilometry, X-ray diffraction, and scanning electron microscopy were employed to characterize the corroded API X 80 steel surfaces. The results showed that the corrosion rate of API X80 steel increased with increasing temperature. Pitting corrosion was observed at lower temperatures, while cracks and sulfide layers of mackinawite and cubic FeS were observed on the corroded steel surface as the temperature increased. Displacement of iron oxide film with a non-protective iron sulfide film was found to be responsible for the pitting corrosion of the API X80 steel.

Keywords: API X80 steel, corrosion, pitting, H₂S, potentiodynamic polarization, profilometry.

1. INTRODUCTION

The presence of H₂S in both natural gas and crude oil has resulted in restricted selection of steel pipelines material used in petroleum product transportation due to corrosion involved [1-3]. The pipeline steels are often susceptible to severe corrosion or combined action of erosion-corrosion [4-7]. Industries have continued to develop new higher strength steels with the aim of identifying materials that can withstand the prevailing corrosive environments [3, 8, 9]. To address this objective, higher grades of carbon steels with improve strength and good corrosion resistance have been developed [9-11]. API X80 steel is considered one of these higher strength steel materials that are widely used as pipeline material for crude oil and natural gas transportation. Regrettably, corrosion of some of these

higher strength steels is often observed [12-14]. Hence, better understanding of the corrosion mechanisms of the API X80 steel is required, especially in sulfide environment.

Corrosion of carbon steel pipelines can occur in different forms [15, 16]. Studies have shown that natural gas, crude oil, industrial waste discharge, and bacteriological process in the seawater contain significant quantities of hydrogen sulfide which affect the integrity of carbon steel [17, 18]. Amongst all, the main source of sulfide is aqueous solution through industrial waste and biological process.[19]. The sulfide attacks materials through physical and chemical nature of the products resulting from their metabolism process [20, 21]. Hydrogen-induced cracking, sulfide stress cracking, and stress-oriented hydrogen induced cracking have been identified as primary sources of pipeline materials failure in sulfide environment [22].

The sulfide corrosion of the carbon steel can be protective or non-protective depending on the environmental conditions and formed corrosion products [18, 23]. These corrosion products are often weak and influenced by iron dissolution and atomic hydrogen diffusion [24, 25]. A recent study by Sherar et al. [15] on the corrosion of API X65 carbon steel in aqueous solution containing NaHCO_3 and Na_2SO_4 as electrolyte showed that a switch from aerobic to aerobic-with-sulfide corrosion significantly increased the relative corrosion rate. Another attempt made by Ma et al. [26] using AC impedance and steady-state polarization curves to study the anodic dissolution of iron in sulfuric acid solutions with H_2S , showed that H_2S can increase both the anodic dissolution and cathodic hydrogen evolution. In another study, Ma et al. [24] studied the inhibition effect of H_2S on iron corrosion. The results revealed that the inhibition property exhibited by H_2S was due to formation of FeS protective film on the electrode surface.

Formation of sulfide layers on the steel surfaces as a corrosion product is often influenced by pH, temperature and exposure time [24, 27]. Yin et al. [28] studied the effect of temperature on the corrosion products formed on carbon steel exposed to a CO_2 -containing solution. The results revealed that increasing the temperature increased the corrosion rate of carbon steel. In a similar study, Qi et al. [29] studied the effect of temperature on the corrosion behavior of flange forging A350LF2 steel. Their results showed that the maximum corrosion rate occurred at 40°C and gradually decreased as the temperature was increased. Despite the several attempts to understand the corrosion behavior of high carbon steel grade [27, 30], only few studies have investigated the corrosion behavior of these steel materials in sour environment [31, 32], especially at low temperature. To the author's knowledge, there is no literature related to the understanding of the corrosion mechanism of API X80 steel in the temperature range and sour environment considered in this study. Understanding of corrosion behavior of API X80 steel in moderate temperature and sulfide environment is important, as this phenomenon accounts for greater percentage of losses incurred in the petroleum industry. Detailed knowledge of H_2S corrosion mechanisms of API X80 steel is not yet clear. Furthermore, general understanding of the sulfide layer formation on surface of the newer higher carbon steel grades used as pipeline material is lacking, especially for the moderate temperatures prevailing in most coastal regions. Therefore, this study investigates the effect of temperature on corrosion of API X80 steel in sulphide environment.

2. EXPERIMENTAL PROCEDURE

2.1 Material

A commercial API X80 pipeline steel purchased from Hebei Yineng Pipeline Group Co., Ltd, China was used in this study. The chemical composition of studied steel is listed in Table 1.

Table 1. Chemical composition of API X80 steel (wt. %)

Element	C	Mn	P	S	Cr	Mo	Ni	Cu	V	Fe
wt. %	0.214	0.522	0.020	0.005	0.043	0.001	0.018	0.014	0.028	Bal.

The specimens for corrosion tests were cut in a cylindrical form of 20mm in length and 15mm in diameter. Before each test, the specimens were ground on 320, 600 and 1200 grit carbon silicon papers, degreased with ethanol, washed with water and then dried in air in order to remove impurities and oxides from the surface.

2.2 Electrochemical measurement tests

All experiments were conducted in a special device glass cell at various temperatures (20, 30, 40, 50 and 60°C) using a GAMRY 600 potentiostat/galvanostat/ZRA. Open Circuit Potential (OCP) was monitored until it became stable. Potentiodynamic polarization (PDP) and electrochemical impedance spectroscopy (EIS) tests were performed following stable OCP profiles for each condition. The test solution was 3.5% of NaCl as a baseline testing environment for all experiments. API X80 steel under investigation was used as the working electrode while graphite was used as the counter electrode. A saturated calomel electrode (SCE, +0.241 V_{SHE}) isolated in a salt bridge and in contact with the polarized electrode was selected as the reference electrode. The specimens were embedded in the glass cell and cross sectional area of 0.785cm² was exposed to electrolyte contact. A deoxygenating process was carried out prior to the introduction of H₂S into the test solution.

For polarization tests, the samples were placed in an open circuit condition for 1hour to stabilize the OCP. The potentiodynamic potential was swept at a scan rate of 0.16mV/sec between -0.15V to 0.5V after steady state open circuit potential was reached. H₂S gas was then continuously bubbled into the solution and a positive pressure of 0.5MPa was maintained for the entire test duration using a flow meter. A Julabo F12 thermostat was used to heat up the temperature of the solution to the desired temperature and maintain the temperature throughout the duration of the tests. AC disturbance signal of 10mV, frequency range between 0.00001 - 20 KHz, and sampling acquisition rate of 10 points/decade were used in the tests. A JENWAY 3510 pH meter was used to measure the pH of each test solution prior and after each test. The actual concentration of H₂S in the solution after the test was determined by iodometric titration method as specified in NACE standard [33].

Field-emission scanning electron microscopy (SEM, FEI NOVA NANOSEM 450, Netherlands) coupled with energy dispersion X-Ray analysis (EDX), were applied to examine the morphology of the corroded samples. D8 Focus Bruker diffractometer X-ray diffraction (XRD) was used to characterize the corrosion layers formed on the API X80 steel specimens after potentiodynamic tests at different temperatures.

3. RESULTS AND DISCUSSION

The initial test medium consists of 3.5% of NaCl solution at 20°C temperature. Introduction of H₂S into the solution at different temperatures of 30°, 40°, 50°, and 60°C significantly shifted the medium more into the acidic region as displayed in Fig.1.

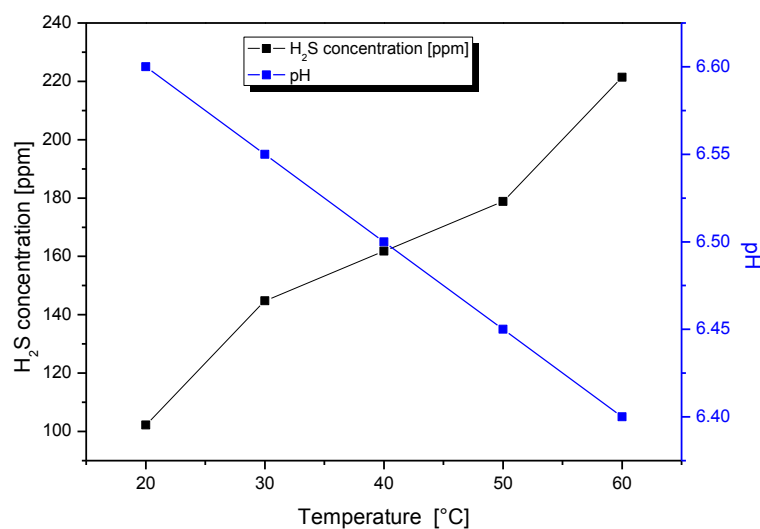


Figure 1. pH variation at different temperatures.

Increasing the temperature of the solution resulted in an increase in the concentration of H₂S in the solution, due to the increase in the rate of chemical reaction; thereby increasing the acidity of the solution. Many studies in the literature have revealed that pH plays a significant role on the corrosion rate of materials in different conditions [1, 2, 34]. Manfredi et al. [35] classified the corrosion behavior of carbon steel using polarization into acidic, neutral and alkaline based on the pH of medium solution. As expected, bubbling of the H₂S into the solution decreased the pH level of the solution and may affect the corrosion mechanism of the API X80 steel under investigation.

3.1 Electrochemical impedance spectroscopy (EIS)

EIS technique was used to study the resistance ability of the API X80 steel to corrosion at different temperatures of 20°, 30°, 40°, 50° and 60°C. Nyquist curves of specimens immersed in 280

mg/L containing 3.5% NaCl bubbled with H₂S at various temperatures are shown in Fig. 2a. It was observed that both real and imaginary impedances decreased with increasing temperature from 20°C to 60°C.

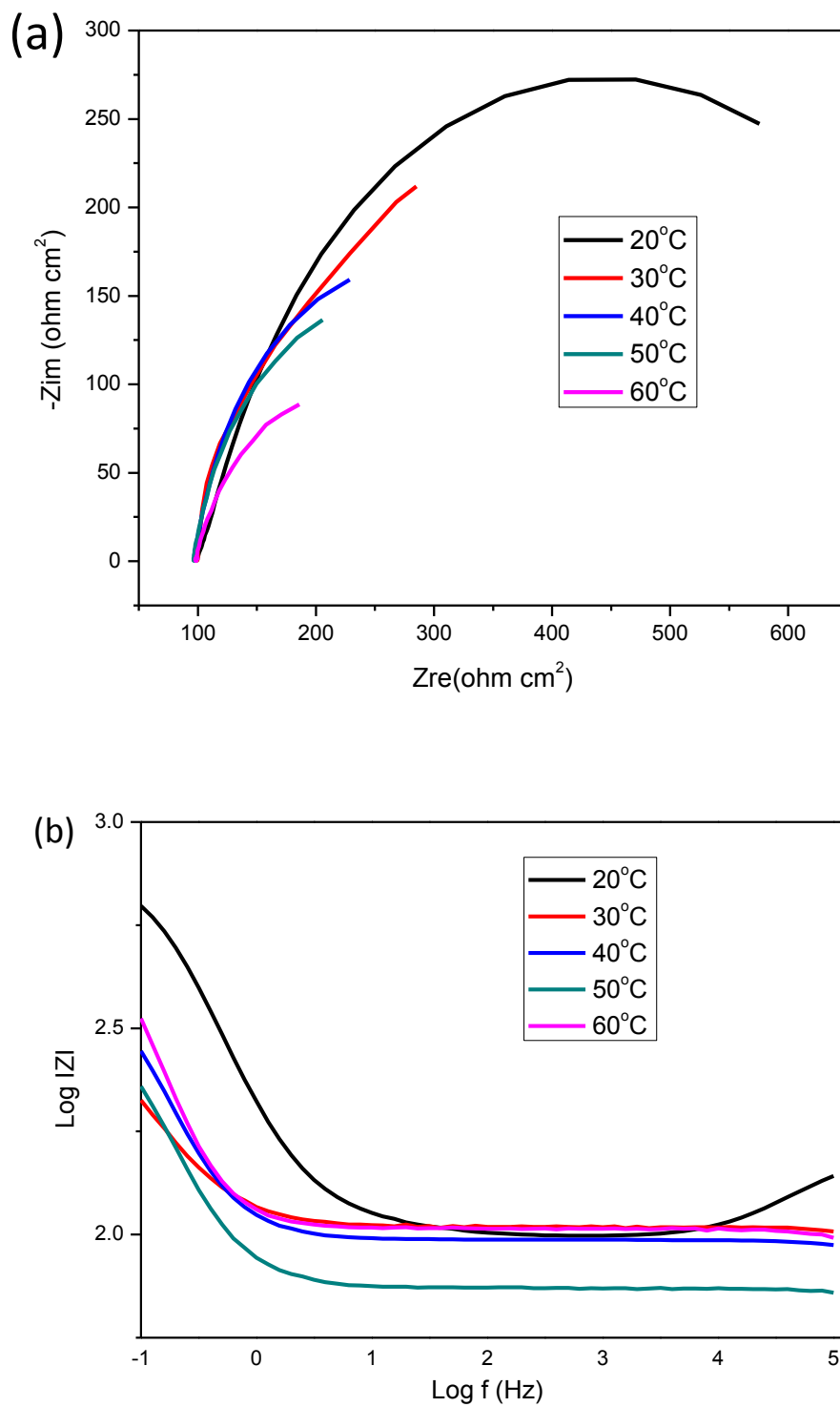


Figure 2. Nyquist and (b) Bode plots of API X-80 steel for different temperatures.

There is a distinct trend in the overall shape of the plots as the temperature of the solution was increased. At 20°C, the Nyquist plot of the steel (Fig.2a) displays a defined single semicircular shape. The test conducted at 30°C showed a decrease in semicircular shape of the curve. When the temperature of the solution was increased to 40 and 50 °C, resistance of 210 and 200 ohms were observed, respectively, which shows a further decrease in the corrosion resistance. Moreover, when the temperature of the solution was increased to 60°C, the resistance of the sample decreased to 150 ohms. It is evident to conclude that corrosion resistance of the API X80 steel significantly decreased as the temperature was increased in such media. This observations is in a good agreement with the published work on SAE-1020 carbon steel subjected to sour environment [36]. Bode plots were also employed to study the corrosion behavior of API X80 steel in H₂S environment at different temperatures, as shown in Fig.2b. The results showed that the corrosion resistance of the specimens gradually decreased by increasing the temperature of the solution. It can be seen that the phase angles tend toward zero at low frequency which indicate the appearance of corrosion products on the specimens [37].

3.2 Potentiodynamic polarization (PDP)

To assess the influence of H₂S and temperature of API X80 steel immersed in NaCl Solution, PDP scans were conducted. Table 2 shows measured values of the corrosion potentials (E_{corr}), Tafel slopes (b_a and b_c represent anodic and cathodic, respectively) and corrosion currents (i_{corr}) obtained from the polarization curves in the 3.5% of NaCl solution bubbled with H₂S at different temperatures. The E_{corr} and i_{corr} were calculated using the Tafel extrapolation method described elsewhere [38].

Table 2. Corrosion parameters obtained from potentiodynamic polarization curves

Temperature (°C)	i_{corr} (mA cm ⁻²)	E_{corr} (V)	Beta A (V dec ⁻¹)	Beta C (V dec ⁻¹)
20	-4.95	-0.9400	0.1215	0.5047
30	-4.82	-0.8930	0.1218	0.4208
40	-4.60	-0.8940	0.1140	0.3403
50	-4.51	-0.8980	0.1190	0.2394
60	-4.37	-0.8960	0.1185	0.1890

It can be seen that the values of b_a (anodic Tafel slopes) shown in Table 2 are closed with ~ 0.12 V per decade for all experiments, regardless of the temperature of the solution. This observation indicated that the temperature of the solution has less significant influenced on the anodic process, while the slopes of the cathodic branch, b_c (Table 2), are significantly depended on the temperature of the solution.

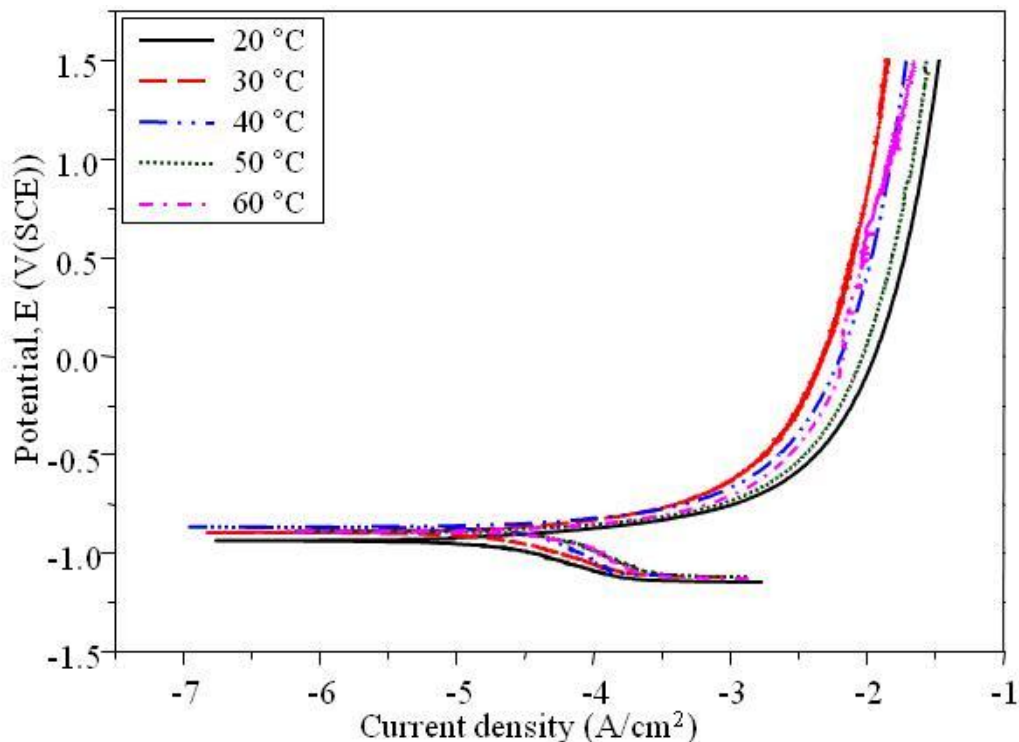
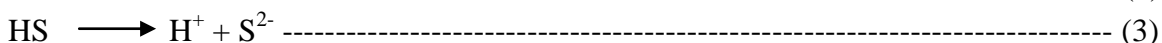


Figure 3. PDP curves of API X80 steel immersed in NaCl solution bubbled with H₂S at different temperatures.

Figure 3 shows the linear polarization behavior of API X80 steel material in 3.5% of NaCl solution bubbled with H₂S at different temperatures. Potentiodynamic polarization was also used to investigate the corrosion rates of the API X80 steel in different hydrogen sulphide solutions at different temperatures. It can be seen that the test conducted at 20°C has the low corrosion rate compared to other temperature tests, as shown in Fig.3. However, the corrosion rate of the sample increased when the temperature of the solution bubbled with H₂S for 1 hour was increased to 30°C. The increased in current density can be attributed to the increase in the pitting mechanism observed on the steel surface at this test condition. At 40°C, the increase in the corrosion rate was evident (Fig.3). These results are in good agreement with the previous finding of Hamdy et al.[23], that revealed that the presence of soluble sulphide in sulphide medium may be responsible for the overall increasing corrosion rate.

It can be seen that hydrogen permeation into 3.5%NaCl solution continued to increase as the temperature increased to 50°C. The same results were observed at 60°C. According to John et al. [2], the overall increase in corrosion rate of the specimens immersed in 3.5% NaCl solution can be attributed to H₂S dissociation into H⁺ and HS⁻ which enhances anodic dissolution process at steel surface (equations 1-3).



This process is also assisted by cathodic hydrogen evolution which accelerates steel oxidation [39]. It may be concluded that the corrosion current density (*i_{corr}*) and corrosion rates increased with increasing H₂S concentration and temperature.

3.3 X-ray diffraction (XRD)

Figure 4 shows the XRD patterns of the API X80 steel specimens after potentiodynamic tests at different temperatures. In order to observe the spectral peaks in the tested samples, scanned range from 20° to 100° and a step width of 0.02° were used in the analysis. The test conducted at 20°C temperature (Fig.4), shows two peaks typical of common carbon steel [40]. Using the ambient temperature test as a reference, key quantitative measurements were obtained from each of the profiles. The results show that the corrosion product layers was composed of iron sulfide at 30°C, 40, 50, and 60°C temperatures. Although no sulfide corrosion peak was detected at 20°C, iron oxide products are generated at this temperature conditions. However, when the temperature of solution was increased to 30°C, different crystallographic planes of iron oxides and iron sulfide were found (Fig.4). It can be seen that Mackinawite has formed on the API X80 steel when the temperature of the solution was increased to 30°C. These results are in consistent with the Nyquist plots shown in Fig.2a, where the steel sample resistance to corrosion dropped significantly as the temperature was increased to 30°.

Closer examination of the general shape of the XRD pattern formed at 40°C revealed similar iron sulfide peak behavior for the 40°C, 50°C and 60°C test temperatures (Fig.4). It has been shown that Mackinawite is the initial product of sulphide formed in the presence of ferrous ions and it is responsible in decreasing the protection potential on metal surface [41]. Shoosmith et al. [1] showed that Mackinawite is formed by both solid-state and precipitation processes with cubic ferrous sulfide and troilite formed as precipitates.

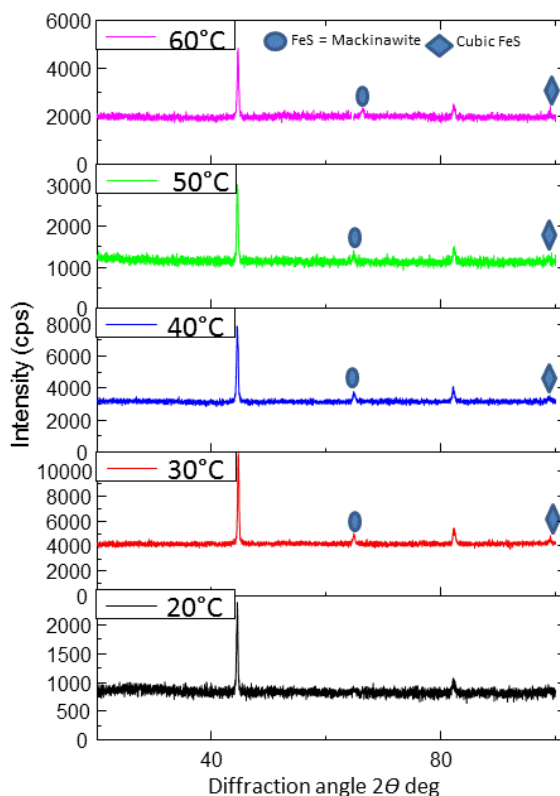
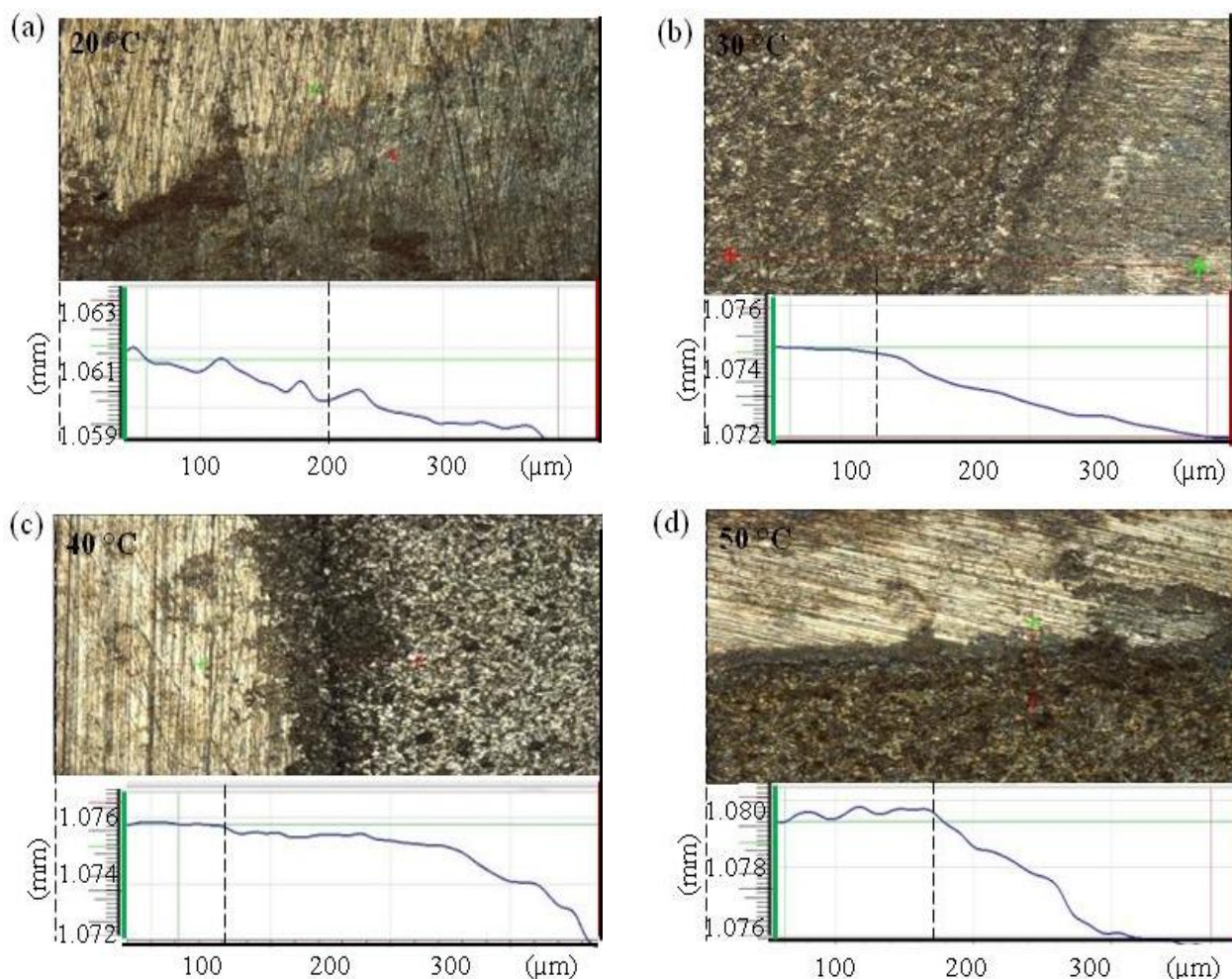


Figure 4. XRD patterns of the API X80 steel conducted at different temperatures.

Their detailed study also revealed that kinetics often necessitates the formation of cubic FeS during short term exposures to sour environment. Their result further showed that temperature plays an important role in the transformation of cubic FeS after its formation either into mackinawite or pyrrhotite at lower or higher temperatures, respectively [1]. Several authors have reported formation of different iron sulfide layers on steel surface at different test conditions [24, 42, 43]. However, most authors believe that Mackinawite is first formed at the electrode surface, which is further transformed into more stable species [44, 45]. The protective nature of the formed sulfide and the composition of the corrosion products significantly depend on the pH, the concentration of H₂S and the temperature of the solution. The metastable mackinawite can transform into other forms of sulfides which are more protective. Furthermore, mackinawite and other sulfide phases such as troilite, pyrrhotite, and pyrite can be formed as corrosion products on the surface of steel depending on the concentration of sulphide present in the solution [46, 47].

3.4 Profilometry analysis



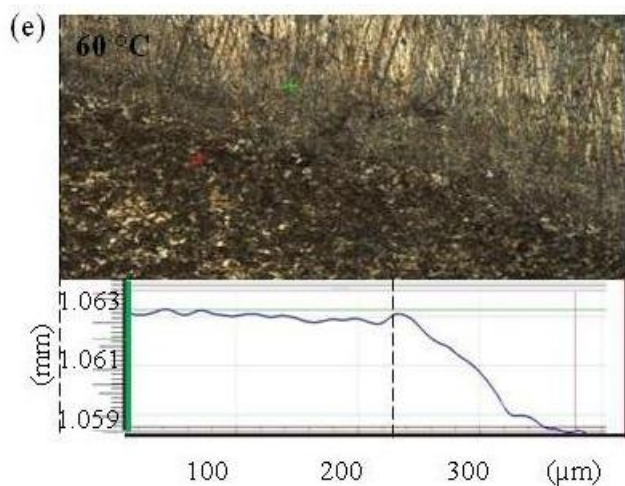


Figure 5. 2D profilometry images of API X80 steel surface at different temperatures.

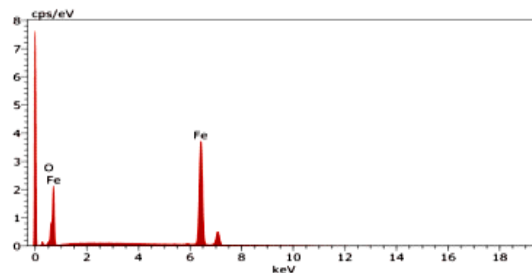
The corrosion scar depth was measured by drawing a profile from a point within the uncorroded surface to the corroded surface of the API X80 steel using a 2D optical profilometry technique, as shown in Fig.5. It is interesting to observe that there is distinct trend in each profile between the uncorroded and corroded surfaces as the temperature was increased. Fig.5a shows the 2D profilometry images of the corroded and uncorroded surface at 20°C temperature test condition. The image shows corrosion scar depth of approximately 0.001mm at this temperature test condition. At 30, 40°C and 50°C temperature test, the corrosion scar increased to 0.002, 0.003 and 0.0035 mm, as shown in Figures 5b, 5c, and 5d, respectively. This observation indicates that material removal due to corrosion process increased with increased temperature.

Fig. 5e shows profile drawn across the corroded and uncorroded surface of the API X80 steel surface after 60°C temperature test. Increased corrosion scar depth is also evident at this test condition. There is obvious increased in the overall slope of the curves as the temperature was increased. This trend indicates possible increase in the severity of the prevailing corrosion mechanism or existence of a dormant corrosion mechanism as the temperature was increased [34].

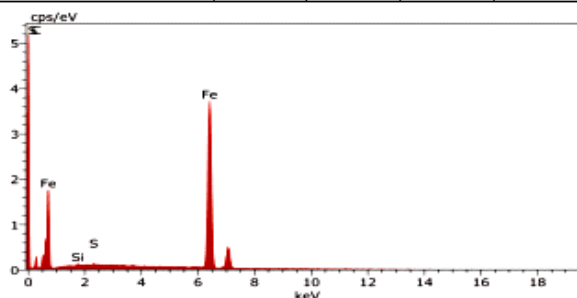
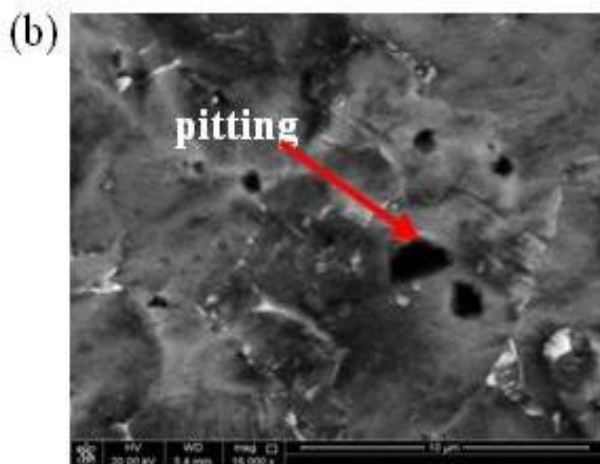
3.5 SEM characterization

The SEM micrographs of the corroded surfaces of the API X80 steel after each corrosion test are shown in Fig.6.

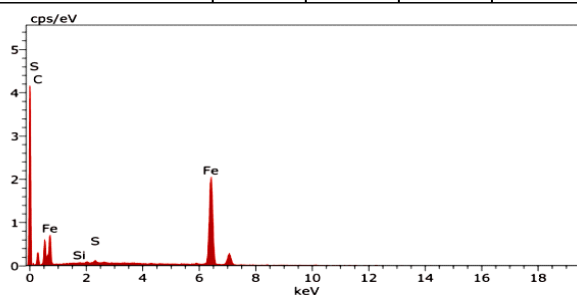
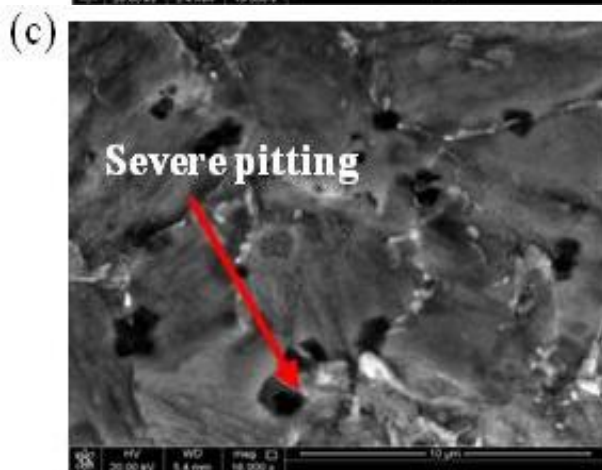
The SEM results reveal that the surfaces of steel samples were corroded at all test temperatures. At 20°C, a relatively rough surface with corrosion products was observed as shown in Fig 6a. When the test temperature was increased to 30°C, pits located across the entire surface of API X80 steel surface were observed. This could be attributed to decrease in the corrosion scar depth observed at this test condition (Fig.5b).



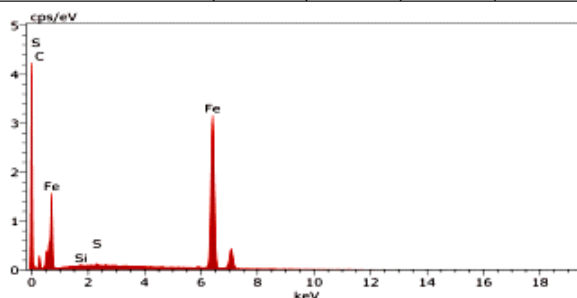
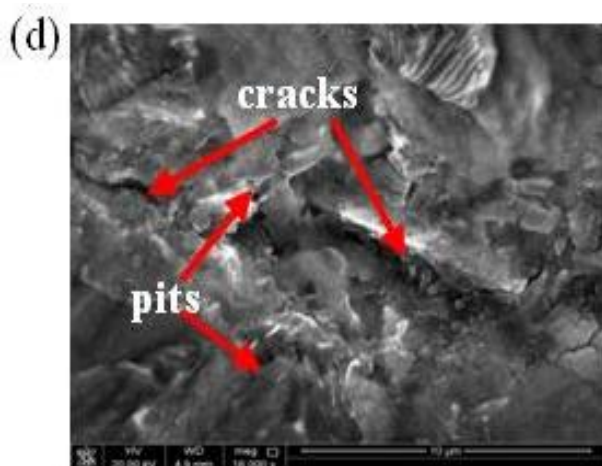
Element	wt. %			
C 6 K - series	07.5	07.3	26.9	2.1
Fe 26 K - series	94.0	92.7	73.1	2.6
Total	101	100	100	



Element	wt. %			
C 6 K - series	11.8	12.9	40.4	2.4
S 16 K - series	00.8	00.9	01.0	0.1
Cl 17 K - series	00.5	00.5	00.5	0.1
Fe 26 K - series	78.9	85.8	58.1	2.2
Total	92.0	100	100	



Element	wt. %			
C 6 K - series	12.0	12.7	39.9	1.91
S 16 K - series	01.5	01.6	01.9	0.08
Si 17 K - series	00.1	00.1	00.1	0.03
Fe 26 K - series	81.2	85.7	58.2	2.19
Total	94.8	100	100	



Element	wt. %			
C 6 K - series	14.5	14.7	44.4	2.15
S 16 K - series	00.1	00.1	00.1	0.03
Si 17 K - series	00.1	00.1	00.1	0.03
Fe 26 K - series	84.2	85.2	55.4	2.26
Total	98.9	100	100	

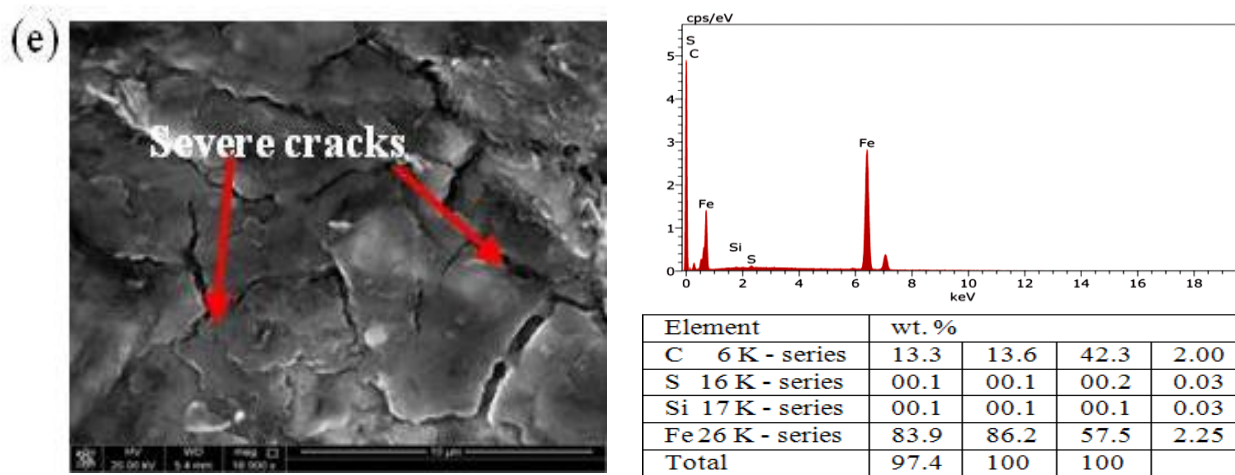


Figure 6. SEM micrographs of the corroded API X80 steel samples at (a) 20°C, (b) 30°C, (c) 40°C, (d) 50°C and (e) 60°C.

These pits appeared to be formed at the white ferrite orientation. The pitting corrosion further increased when the temperature was increased to 40°C (Fig.6c). It is evident that the number of pits observed on the API X80 steel at 40°C is more than that of 30°C. Hamdy et al. [23] reported that presence of sulfur could be responsible for the corrosive attack resulting from local acidification of iron sulfide formation. The results further revealed that localized replacement of protective iron oxide film by non-protective iron sulfide film may be responsible for the formation of pitting corrosion observed between 30 and 40°C. The micropits observed on the API X80 steel surface offer ‘transfer tunnel’ for aggressive species in bulk solution, which enhances the solution species to readily penetrate the metal surface, leading to an increase in the corrosion rates. This results in material removal of the sample surface through corrosion process as observed in this study. The EDX analysis of the corroded API X80 steel surface at 30 and 40°C temperature tests shows evidence of this sulfur element (Figs.6b and 6c). It therefore becomes obvious that the presence of sulfur contributed to the pitting mechanism observed in this study. It is clear that the pits formed on the API X80 steel surface (Figs.6b and 6c) belongs to the first iron sulfide product layer type as was shown in the XRD results (Fig.4).

Fig.6d clearly shows that sulphur layers formed on the API X80 steel increased as the temperature was increased to 50°C. However, examination of the corroded surfaces at 50 and 60°C shows that the corroded surface exhibits some cracks on the sample surface which is in close agreement with the increasing corrosion scar depth trend observed as the temperature was increased (Fig.5). It is well known that the pitting corrosion is one of the main potential sites for surface crack formation. This indicates that increasing the temperature to 50°C resulted in the change from pitting to crack formation on the API X80 steel surface, as seen in Fig.6d. Increasing the temperature of the solution to 60°C also showed that cracking of the API X80 steel surface was a dominant corrosion mechanism. Increase in the stress concentration in the pit will result in possible crack nucleation and subsequent propagation as observed in this study. There is a notable change in the cracks for the 60°C tests, when compared to the 50°C tests. The corroded surface of the API X80 steel at 60°C temperature test shows obvious large cracks on the sample surface compared to that of 50°C temperature test and could be attributed to increasing temperature effect on the sulfide formation (Figs.6d and 6e). It is clear

from the EDX analysis that Fe/S ratio slightly decreased with increasing temperature, indicating increasing concentration of sulfur with temperature. With respect to potentiodynamic data in Table 2 and Fig.6, it could be seen that the pitting corrosion increased with increase temperature from 30 to 40°C, whereas hydrogen-induced cracking was a predominant mechanism at 50 and 60° temperatures.

4. CONCLUSIONS

The corrosion behavior of API X80 steel was investigated in 3.5% of NaCl solution bubbled with H₂S at temperature range of 20°C - 60°C, using potentiodynamic, EIS, XRD, profilometry and SEM techniques were used to characterize the corrosion mechanism. The following conclusions may be drawn:

1. There is a significant increase in corrosion rates of API X80 steel immersed in NaCl solution and in the presence of H₂S. Formation of corrosion pitting and hydrogen induced cracking occurred at lower and higher temperatures, respectively.
2. Combined observations using XRD, SEM and EDX showed the presence of iron sulfide at different temperatures above the 20°C temperature.
3. The increase in the corrosion rate was attributed to the formation of iron sulfide layers on the API X80 steel surface which builds up, cracks, breaks up and re-builds as more H₂S was introduced in the solution.
4. Profilometry analysis showed that corrosion of the API X80 steel resulted in material removal displayed by the trend in the corrosion scar depth profile as the temperature was increased.

ACKNOWLEDGEMENT

This publication was made possible by NPRP Grant 6-027-2-010 from the Qatar National Research Fund (a Member of The Qatar Foundation). The statements made herein are solely the responsibility of the authors.

Reference

1. D. W. Shoesmith, M. Peter Taylor, G. Bailey. and D. G. Owen., *Electrochemical Society*, 127 (1980) 1007.
2. J. W. Morse, F. J. Millero, J. C. Cornwell and D. Rickard, *Earth-Science Reviews*, 24 (1987) 1.
3. J. B. Choi, B. K. Goo, J. C. Kim, Y. J. Kim and W. S. Kim, *International Journal of Pressure Vessels and Piping*, 80 (2003) 121.
4. M. Aminul Islam, Z. N. Farhat, E. M. Ahmed and A. M. Alfantazi, *Wear*, 302 (2013) 1592.
5. P. C. Okonkwo and A. M. A. Mohamed, *International Journal of Engineering Science and Innovative Technology (IJESIT)*, 6 (2014) 3.
6. C. Okonkwo Paul and C. Adel M, Mohamed., *International Journal of Metallurgical & Materials Science and Engineering (IJMMSE)*, 4 (2014) 7.
7. R. Malka, Erosion Corrosion and Synergistic Effects in Disturbed Liquid-Particle Flow, in, *Ohio University*, 8 (2005) 17.
8. K. Junhua, Z. Lin, G. Bin, L. Pinghe, W. Aihua and X. Changsheng, *Materials & Design*,

- 25 (2004) 723.
9. H.C. ASM International, steels, and high-performance alloys. Metals Parks, Ohio: *American Society for Metals*, 5 (1995) 215.
 10. J. Niu, L.-H. Qi, Y.-I. Liu, L. Ma, Y.-R. Feng and J.-X. Zhang, *Transactions of Nonferrous Metals Society of China*, 19 (2009) 573.
 11. R. Li, X. Zuo, Y. Hu, Z. Wang and D. Hu, *Materials Characterization*, 62 (2011) 801.
 12. J. Sojka, M. Jérôme, M. Sozańska, P. Váňová, L. Rytířová and P. Jonšta, *Materials Science and Engineering: A*, 480 (2008) 237.
 13. J. J. Park, S. I. Pyun, K. H. Na, S. M. Lee and Y. T. Kho, *Corrosion*, 58 (2002) 329.
 14. G. Z. Meng, C. Zhang and Y. F. Cheng, *Corrosion Science*, 50 (2008) 3116.
 15. B. W. A. Sherar, P. G. Keech and D. W. Shoesmith, *Corrosion Science*, 66 (2013) 256.
 16. Y.-S. Choi, S. Nestic and S. Ling, *Electrochimica Acta*, 56 (2011) 1752.
 17. M. B. Kermani and A. Morshed, *Corrosion*, 59 (2003) 659.
 18. J. L. Crolet, N. Thevenot and S. Nestic, *Corrosion*, 54 (1998) 194.
 19. P. N. L. Lens, A. Visser, A. J. H. Janssen, L. W. H. Pol and G. Lettinga, *Critical Reviews in Environmental Science and Technology*, 28 (1998) 41.
 20. O. J. Hao, J. M. Chen, L. Huang and R. L. Buglass, *Critical Reviews in Environmental Science and Technology*, 26 (1996) 155.
 21. W. A. Hamilton, *Annual Review of Microbiology*, 39 (1985) 195.
 22. M. Al-Mansour, A. M. Alfantazi and M. El-boujdaini, *Materials & Design*, 30 (2009) 4088.
 23. A. S. Hamdy, A. G. Sa'eh, M. A. Shoeib and Y. Barakat, *Electrochimica Acta*, 52 (2007) 7068.
 24. H. Ma, X. Cheng, G. Li, S. Chen, Z. Quan, S. Zhao and L. Niu, *Corrosion Science*, 42 (2000) 1669
 25. H. Y. Ma, X. L. Cheng, S. H. Chen, G. Q. Li, X. Chen, S. B. Lei and H. Q. Yang, *Corrosion*, 54 (1998) 634.
 26. H. Ma, X. Cheng, S. Chen, C. Wang, J. Zhang and H. Yang, *Journal of Electroanalytical Chemistry*, 451 (1998) 11.
 27. B. W. A. Sherar, P. G. Keech, J. J. Noël, R. G. Worthingham and D. W. Shoesmith, *Corrosion*, 69 (2012) 67.
 28. Z. F. Yin, Y. R. Feng, W. Z. Zhao, Z. Q. Bai and G. F. Lin, *Surface and Interface Analysis*, 41 (2009) 517.
 29. Y. Qi, H. Luo, S. Zheng, C. Chen, Z. Lv and M. Xiong, *Int. J. Electrochem. Sci*, 9 (2014) 2101.
 30. F. F. Eliyan and A. Alfantazi, *Corrosion*, 70 (2014) 880.
 31. S. Papavinasam, A. Doiron and R. W. Revie, *Corrosion*, 66 (2010) 035006.
 32. N. Sridhar, D. S. Dunn, A. M. Anderko, M. M. Lencka and H. U. Schutt, *Corrosion*, 57 (2001) 221
 33. S. M. Lee, W. G. Lee, Y. H. Kim and H. Jang, *Corrosion Science*, 63 (2012) 404.
 34. C. Manfredi, T. A. Mozhi and B. E. Wilde, *Corrosion*, 45 (1989) 172.
 35. J. Tang, Y. Shao, J. Guo, T. Zhang, G. Meng and F. Wang, *Corrosion Science*, 52 (2010) 2050.
 36. M. A. Arafin and J. A. Szpunar, *Materials Science and Engineering: A*, 528 (2011) 4927.
 37. W. Lee, Z. Lewandowski, P. H. Nielsen and W. A. Hamilton, *Biofouling*, 8 (1995) 165.
 38. H. Tamura, *Corrosion Science*, 50 (2008) 1872.
 39. J. B. Sardisco and R. E. Pitts, *Corrosion* 21 (1965) 245.
 40. A. G. Wikjord, T. E. Rummery, F. E. Doern and D. G. Owen, *Corrosion Science*, 20 (1980) 651.
 41. B. W. A. Sherar, I. M. Power, P. G. Keech, S. Mitlin, G. Southam and D. W. Shoesmith, *Corrosion Science*, 53 (2011) 955.
 42. D. Rickard, Metastable Sedimentary Iron Sulfides, in *Developments in Sedimentology*, 195 (2012) 116.
 43. P. Bai, S. Zheng, C. Chen and H. Zhao, *Crystal Growth and Design*, 14 (2014) 4295.
 44. A. N. Buckley and R. Woods, *Applied Surface Science*, 27 (1987) 437.

45. I. C. Hamilton and R. Woods, *Journal of Electroanalytical Chemistry and Interfacial Electrochemistry*, 118 (1981) 327.

© 2015 The Authors. Published by ESG (www.electrochemsci.org). This article is an open access article distributed under the terms and conditions of the Creative Commons Attribution license (<http://creativecommons.org/licenses/by/4.0/>).